Effects of atomic short-range order on properties of the PbMg_{1/3}Nb_{2/3}O_{3} relaxor ferroelectric

Sergey Prosandeev and L. Bellaiche

Phys. Rev. B **94**, 180102 — Published 3 November 2016

DOI: 10.1103/PhysRevB.94.180102

Effects of atomic short-range order on properties of $Pb(Mg_{1/3}Nb_{2/3})O_3$ relaxor ferroelectric

Sergey Prosandeev[1,2] and L. Bellaiche[1]

[1] *Physics Department and Institute for Nanoscience and Engineering, University of Arkansas, Fayetteville, Arkansas 72701, USA*

[2] *Institute of Physics and Physics Department of Southern Federal University, Rostov-na-Donu 344090, Russia*

Abstract

The effect of atomic *short-range* order on macroscopic and microscopic properties of the prototype of relaxor ferroelectrics, that is lead magnesium niobate $Pb(Mg_{1/3}Nb_{2/3})O_3$ (PMN), is studied via the combination of an annealing technique and a large scale effective Hamiltonian method. The investigated short-range order gradually varies from the case of fully disordered solid solutions to the situation for which the first three nearest neighboring shells of the B lattice of PMN adopt a rocksalt ordering between a sublattice made of pure Nb ions and a randomly distributed sublattice consisting of 2/3 of Mg and 1/3 of Nb. Characteristic temperatures of relaxor ferroelectrics (namely, the Burns, so-called T^* and depolarizing temperatures) significantly increase when strengthening this short-range chemical order, which is accompanied by an overall enhancement of the size of the polar nanoregions as well as of some antiferroelectric interactions. These results can be understood by the fact that chemical short-range order strongly modifies the internal electric fields felt by the Pb ions.

Relaxor ferroelectrics form an important class of disordered materials that are characterized by large and strongly frequency-dependent dielectric permittivity as well as by several unusual characteristic temperatures [1, 2], with these compounds remaining macroscopically paraelectric down to 0K. One of these characteristics temperatures is the famous Burns temperature [3], at which it is commonly believed that relaxor ferroelectrics begin to acquire polar nanoregions that are responsible for their anomalous properties. Another temperature is often denoted as T^* and is associated with an anomaly in acoustic emission and in the temperature dependence of the lattice constant, and with striking features in the Raman and neutron scatterings [4–9]. A third characteristic temperature is the depolarizing temperature, at which the poled relaxor system looses its polarization on heating [10–13]. Relaxor ferroelectrics continue to attract attention in order to fully understand their unusual properties, as, e.g., demonstrated by recent computational studies shedding new light into them (see, e.g, Refs. [14–19] and references therein).

It is also important to realize that the theory of (classical) ferroelectrics typically considers the long-range electrostatic interactions as the main cause of ferroelectricity [20], and that such latter interactions can be modified in relaxors by, e.g., the simultaneous presence of both ferroelectrically active and inactive ions inside these systems [21, 22] or by the existence of the so-called random electric fields [10] or random strains originating from the difference in charge and size, respectively, of the mixed ions. As a result, one may dramatically alter characteristic temperatures of relaxor ferroelectrics if one can vary these random fields. One way to change them is to modify the *long-range* chemical ordering between the mixed ions, as experimentally found (by changing the growth conditions) and theoretically predicted in, e.g., Refs. [23, 24] for $PbSc_{1/2}Ta_{1/2}O_3$ and $PbSc_{1/2}Nb_{1/2}O_3$ systems, when going from disordered to long-range rocksalt-ordered structure.

However, several relaxor ferroelectrics, including the prototype lead magnesium niobate $Pb(Mg_{1/3}Nb_{2/3})O_3$ (PMN), do not present a long-range ordering between the mixed ions but rather possess a chemical order of short-range nature, as, e.g., evidenced by the small intensity of X-Ray superstructure peaks found in Refs. [25, 26]. Strikingly, the effect of chemical short-range order on properties of relaxor ferroelectrics is not well-known. For instance, it is not clear if and how short-range chemical order can affect macroscopic and local properties of relaxor ferroelectrics, and if the (hypothetical) variation of these quantities can be understood at a microscopic level. One reason for this paucity of knowledge is that

it is difficult to experimentally extract the amount (and type) of short-range order present in a relaxor ferroelectric. Another reason is that simulating short-range order is not a straightforward task since one needs to mimic very specific short-range atomic correlations, which also requires the use of large supercells.

The aims of this Letter are to provide the answers to these issues, by combining an annealing technique and an effective Hamiltonian scheme, and to reveal that not only many properties of PMN strongly depend on chemical short-range order but also that these dependencies are linked to the internal electric fields felt by the Pb ions.

Here, the effect of short-range order on properties of PMN is investigated by first considering $18 \times 18 \times 18$ supercells made of the virtual $Pb(Nb_{0.5} < B_{av} >_{0.5})O_3$ solid solutions, where $< B_{av} >$ is an artificial atom made of 2/3 of Mg and 1/3 of Nb. Chemical ordering of this $Pb(Nb_{0.5} < B_{av} >_{0.5})O_3$ system is then introduced via the concept of the Cowley parameters [27–30] that are defined as:

$$\alpha_j = 1 - 2P_j \tag{1}$$

where P_j is the probability of finding a Nb (respectively, $< B_{av} >$) atom being the jth nearest neighbor of a $< B_{av} >$ (respectively, Nb) atom in the mixed B sublattice. Here, we practically consider j=1, 2 and 3 (that is the first, second and third nearest neighbors' shells of the B-sublattice) and impose $\alpha_1 = -\alpha$, $\alpha_2 = +\alpha$ and $\alpha_3 = -\alpha$, with α varying between +0.0 (which characterizes perfect disorder between the Nb and $< B_{av} >$ ions) and +1.0 (which corresponds to Rock-Salt-ordering of the first three neighboring shells between the Nb and $< B_{av} >$ ions) by step of 0.1. Such procedure is technically performed via an annealing method [30] aiming to reach the desired values of α_1, α_2 and α_3, and therefore leads to the generation of 11 different supercells, each associated with its own α and thus representative of different short-range chemical orderings (note that we numerically found that imposing α_1=-1, α_2=+1 and α_3=-1 results in fact in the long-range atomic ordering of Rock-Salt type of *all* the shells, that is the corresponding configuration adopts the long-range rocksalt-ordering in addition to a short-range rocksalt-ordering; note also that we did not consider here the existence of rocksalt-ordered regions existing inside a disordered matrix as in Refs. [16, 17]). For each of these 11 supercells, we then use a *random* number generator to replace the virtual $< B_{av} >$ atoms by real Mg and Nb ions in 2:1 proportion. Note that we practically use 30 different random numbers, which effectively results in the generation

of 30 different configurations for any considered α. The properties of these 30 configurations are then averaged in order to better mimic the disorder inherent to the $< B_{av} >$ sublattice (note that such procedure for $\alpha = +1$ is consistent with the so-called "random site" model of PMN [25, 26] that is characteristic of a $1:1$ chemical order, inside which pure Nb planes alternate along the [111] pseudo-cubic direction with planes containing a random mixture of 1/3 of Nb and 2/3 of Mg ions).

The atomistic effective Hamiltonian of Ref. [31] is then employed to model the effect of these chemical orders on properties of PMN by using all the aforementioned constructed supercells within Monte-Carlo simulations. Its degrees of freedom are (1) the local modes, $\mathbf{u_i}$, at each 5-atom unit cell i and that are centered on Pb ions (these local modes are directly proportional to local electric dipoles); and (2) the homogeneous and inhomogeneous strains. More details about this effective Hamiltonian is given in the Supplemental Material [31–34].

Figure 1a shows the predicted averaged diagonal component of the dielectric tensor, χ (i.e., 1/3 of the trace of this tensor), as a function of temperature for the investigated short-range-order parameters. Such dielectric response adopts a broad peak for any considered α, as characteristic of relaxor ferroelectrics [1, 2]. This broad peak is centered around a temperature that depends on the amount of short-range ordering, that is about 350-400K for $\alpha = 0$ *versus* about 500K for $\alpha = 1$. Results obtained in Ref. [24] for another relaxor ferroelectric, that is $Pb(Sc_{0.5}Nb_{0.5})O_3$, and showing that the diffuse peak of dielectric permittivity shifts to higher temperatures when going from a disordered system to a chemically rocksalt-ordered compound, are therefore also valid for PMN. It is interesting to realize that Ref. [26] also observed that the position and intensity of the dielectric permittivity peak in PMN:Tb changes after thermal annealing at high temperatures, as a result of the emergence of large rocksalt-ordered domains. Note that, as also characteristic of relaxor ferroelectrics, [1, 2], PMN is found to be paraelectric down to the lowest investigated temperatures for any studied α, except for a few configurations that can have non-vanishing polarization below $\simeq$ 300K, especially for larger α. For example, at $\alpha = 1$ and $T = 50$K, there are three configurations with significant polarization among the 30 investigated supercells. On the other hand, the magnitude of the local mode, as averaged over the 30 configurations, is rather small for any α. In other words, PMN can be thought to be paraelectric on average, independently of our studied short-range chemical ordering. Note that the few configurations that exhibit a significant polarization are responsible for the enhancements of the dielectric response (for

which values are above $\simeq$ 2,000) seen in Fig. 1a for temperatures below 300K. Such (anomalous) enhancements indicate that the relaxor and ferroelectric phases are close to each other in energy in PMN, and that the atomic distribution between Nb and Mg ions can alter their energetics. Moreover, Figure 1b reports the *inverse* of χ as a function of temperature. This function can be well fitted by a straight line for temperatures higher than the Burns temperature [3] (to be denoted as T_B in the following), with the interpolation of this straight line with the zero occurring at a temperature that we estimate to be the T^* characteristic temperature of relaxor ferroelectrics [4–9]. Figure 1c reveals the rather strong dependency of T^* on α. For instance, T^* increases from about 397K to $\simeq$ 508K when α varies from 0 to 1. For comparison, different experiments indicated a T^* being close to 350K in Ref. 6, near $T^* = 400$K in Refs. 4, 5, and 8 and as high as 500K in Ref. 7. This observed large variation can therefore be explained by a difference in atomic short-range ordering according to our simulations. Figure 1c further indicates that our computed T_B are less sensitive on α than T^*: It is about 605K at $\alpha = 0$ and 660K at $\alpha = 1$, that is T_B varies by only 9% while T^* is enhanced by about 28% when α increases from 0 to 1. Note that our predicted range for T_B also includes the Burns temperature of 620K reported in Ref. [3] for PMN.

Let us now determine if short-range-ordering in PMN has some effect on the microstructure. For that, we report in the insets of Fig. 2a snapshots of the electric dipolar pattern for a single configuration of two different α parameters, namely $\alpha = 0$ and 1, at 50 K. In these insets, the red lines delimit polar nanoregions (PNRs) inside which the dipoles are nearly parallel to each other, and existing within our $18 \times 18 \times 18$ supercells. These PNRs are determined using the same method as in Ref. [35] and their size is estimated [36] as $s =< N_{PNR}^2 > / < N_{PNR} >$, where N_{PNR} is the number of the sites belonging to a particular polar nanoregion while <> denotes averages over the different PNRs. Figure 2a reports the dependency of s with α (as averaged over the 30 investigated configurations for each α), which reveals that polar nanoregions typically grow in size if one increases the degree of the chemical short-range order – as consistent with the comparison between the left and right insets of this figure. This cluster size nearly doubles in average from 13 to 24 sites when going from the disordered case to the atomic arrangements corresponding to $\alpha = +1$.

Moreover, various studies suggested that antiferroelectricity (AFE) also plays some role in relaxor ferroelectrics [31, 37–39]. To check such fact and determine how such AFE depends on short-range chemical order in PMN, we computed the magnitudes of the Fourier transform

[40] of the x-components of the local modes in the considered supercells [41]. The largest Fourier transforms correspond to the following q-points [42]: $2\pi(n_x, n_y, nz)/18a_{lat}$, where a_{lat} is the 5-atom cubic lattice constant and with (n_x, n_y, nz) = (2,0,-2), (-2,0,2), (-2,2,0), (2,-2,0), (-2,-2,0), (2,2,0), (2,0,2), and (-2,0,-2). Figure 2b reports the dependence of the sum of the magnitudes of these eight largest Fourier transforms on α at 50K, which demonstrates that short-range order has the tendency to also enhance antiferroelectric correlations – in addition to strengthen the size of the PNRs in average (as shown in Fig. 2a). Interestingly, these AFE correlations are not negligible, once realizing that the sum of the magnitudes of the Fourier transforms [40] of the x-components of the local modes on *all* q-points amounts to unity and that the data reported in Fig. 2b varies between $\simeq 0.38$ and $\simeq 0.53$. Note also that both Figs 2a and 2b indicate that this sum as well as the size of the PNRs also strongly depend on the different configurations used for any given α, as demonstrated by the large error bars provided in these figures – which further demonstrates the significant effect of the atomic distribution of Mg and Nb ions on properties of PMN.

In order to have a real-space picture of correlations between electric dipoles, we also computed:

$$\theta_{x,x}(\mathbf{r}) = \frac{1}{N_{Pb}} \sum_i \frac{u_{i,x} u_{i+r,x}}{|\mathbf{u_i}| \, |\mathbf{u_{i+r}}|} \tag{2}$$

where the sum runs over all the N_{Pb} Pb-sites i of the system. $\mathbf{u_i}$ and $\mathbf{u_{i+r}}$ are the local modes in cell i and in the cell centered on the Pb atom distant by $\mathbf{r}$ from cell i, respectively, and $u_{i,x}$ and $u_{i+r,x}$ are their x-components, respectively. The two insets of Fig. 2b display $\theta_{x,x}(\mathbf{r})$ as averaged over the (001) planes, for the same configurations used for the insets of Fig. 2a, for α=0 and 1. These two insets both show (i) ferroelectric correlations (for which $\theta_{x,x}(\mathbf{r})$ is positive) for distances less than $2a_{lat}$ in the (x,y) plane, as consistent with the existence of the (small) polar nanoregions depicted in the insets of Fig. 2a; and (ii) strong antiferroelectric correlations (for which $\theta_x(\mathbf{r})$ is negative and of magnitude of about 0.13 for $\alpha = 0$ and 0.18 for $\alpha = 1$) at, e.g., distances of $4a_{lat}$ and $5a_{lat}$ along the x-axis as well as those deduced from them by translation along the y-axis by $9a_{lat}$. Such AFE is in-line with the significant sum of the Fourier transforms of Fig. 2b and with the predictions of the importance of the antiferroelectric interactions on relaxor properties [37].

We also conducted simulations corresponding to zero field heating (ZFH) after (i) field

cooling (FC) PMN down to 50 K under an electric field of $\sqrt{3}$ 10^8 V/m magnitude and oriented along the [111] direction and (ii) then removing such field before heating the system. As consistent with known features of PMN [10–13], such procedure leads to the formation of a polarization along the [111] direction, that we denote here as P_{ZFH-FC}. Such polarization exists from low temperatures up to a specific temperature, that is typically coined the depolarizing temperature [10–13] and that we will refer to as T_{depol}, above which the systems suddenly reverts to its relaxor state (for which the macroscopic polarization is null). Figure 3 shows the behavior of P_{ZFH-FC} *vs.* temperature for different α which, e.g, allows us to extract the dependency of two different quantities on short-range order: (i) T_{depol}, which is displayed in Fig. 1c (along with T^* and T_B); and (ii) P_{ZFH-FC} calculated at our lowest investigated temperature of 10K, which is reported in the inset of Fig. 3. Both T_{depol} and P_{ZFH-FC} at 10K increase with α, which indicates that short-range-order clustering has the tendency to deepen the energy well of the ferroelectric phase in addition to move it to larger polarization at low temperature. Note that T_{depol} in our calculations changes from 280K $\pm$ 10K at $\alpha = 0$ to 459K $\pm$ 10K at $\alpha = 1$, while data of about 210K were reported in Ref. 11.

With the aim to understand the origin of the aforementioned striking dependency of the macroscopic and local properties of PMN on the degree of the chemical order, we further calculated the internal electric field, $\mathcal{E}_\mathbf{i}$, felt by each Pb ion (and due to the difference in charges between Nb and Mg ions) in our 18x18x18 supercells (see the Supplemental Material and Refs. [16, 31, 33, 43, 44] for details about this calculation). An averaged magnitude of internal electric fields is then defined as $E_{internal} = \sqrt{\frac{1}{N_{Pb}} \sum_i \mid \mathcal{E}_\mathbf{i} \mid^2}$. Figure 1d shows such magnitude and reveals that $E_{internal}$ decreases as α increases. As shown in the inset of Fig. 1d, this decrease is linearly correlated (and thus explains) the concomitant enhancement of the T^*, T_B, and T_{depol} temperatures with α. One can thus safely conclude that properties of PMN are strongly linked to their internal electric fields, as consistent with Refs [10, 16, 31, and 45]. In particular, Ref. [31] predicted that the full (but unpractical) annihilation of internal electric fields inside PMN would result in a ferroelectric ground state, which is consistent with the fact that T_{depol} is the highest, and also the closest to T^*, when $\alpha = 1$ in all our investigated short-range ordered configurations.

In summary, we demonstrated that chemical short-range order can highly affect macroscopic properties of PMN, such as the diffuse dielectric permittivity peak position, the polarization in its field-induced ferroelectric phase as well as the Burns, T^* and depolarizing

temperatures. Such ordering has also an overall effect on microscopic quantities, such as the size of the polar nanoregions and antiferroelectric interactions. These effects originate from the fact that varying the chemical short-range order is one effective way to alter the internal electric fields felt by the Pb ions. We therefore hope that this manuscript helps in better understanding complex solid solutions, in general, and relaxor ferroelectrics, in particular. It can also motivate the study of chemical short-range order on properties not studied here, such as dielectric relaxation [18].

This work is financially supported by ONR Grant N00014-12-1-1034. S.P. also appreciates the Russian Foundation for Basic Research (grant 16-52-00072 Bel_a).

[1] L. E. Cross, Ferroelectrics **151**, 305 (1994).

[2] G. A. Smolensky *et al.*, *Ferroelectrics and Related Materials*, (Gordon and Breach, New York 1981).

[3] G. Burns and F. H. Dacol, Phys. Rev. B **28**, 2527 (1983); Solid State Com. 48, 853 (1983).

[4] D. Viehland, S. J. Jang, L. E. Cross, and M. Wuttig, Phys. Rev. B **46**, 8003 (1992).

[5] B. Dkhil, J. M. Kiat, G. Calvarin, G. Baldinozzi, S. B. Vakhrushev, and E. Suard, Phys. Rev. B **65**, 024104 (2001).

[6] O. Svitelskiy, J. Toulouse, G. Yong, and Z.-G. Ye, Phys. Rev. B **68**, 104107 (2003).

[7] B. Dkhil, P. Gemeiner, A. Al-Barakaty, L. Bellaiche, E. Dulkin, E. Mojaev, and M. Roth, Phys. Rev. B **80**, 064103 (2009).

[8] C. Stock, L. Van Eijck, P. Fouquet, M. Maccarini, P. M. Gehring, G. Xu, H. Luo, X. Zhao, J.-F. Li, and D. Viehland, Phys. Rev. B **81**, 144127 (2010).

[9] S. Prosandeev, I. P. Raevski, M. A. Malitskaya, S. I. Raevskaya, H. Chen, C.-C. Chou, and B. Dkhil, J. Appl. Phys. **114**, 124103 (2013).

[10] V. Westphal, W. Kleemann, and M. D. Glinchuk, Phys. Rev. Lett. **68**, 847 (1992).

[11] E. V. Colla, E. Yu. Koroleva, N. M. Okuneva, and S. B. Vakhrushev, Ferroelectrics **184**, 209 (1996).

[12] R. Pirc, Z. Kutnjak, and N. Novak, J. Appl. Phys. **112**, 114122 (2012).

[13] G. Xu, G. Shirane, J. R. D. Copley, and P. M. Gehring, Phys. Rev. B **69**, 064112 (2004).

[14] H. Takenaka, I. Grinberg, and A. M. Rappe, Phys. Rev. Lett. **110**, 147602 (2013).

[15] I. Grinberg and A. M. Rappe, Phys. Rev. B **70**, 220101(R) (2004).

[16] S. Tinte, B. P. Burton, E. Cockayne, and U. V.Waghmare, Phys. Rev. Lett. **97**, 137601 (2006).

[17] P. Ganesh, E. Cockayne, M. Ahart, R. E. Cohen, B. Burton, Russell J. Hemley, Yang Ren, Wenge Yang, and Z.-G. Ye, Phys. Rev. B **81**, 144102 (2010).

[18] D. Wang, A.A. Bokov, Z.-G. Ye, J. Hlinka and L. Bellaiche, Nat. Comm. **7**, 11014 (2016).

[19] Y. Nahas, S. Prokhorenko, I. Kornev, L. Bellaiche, Phys. Rev. Lett. **116** 127601 (2016).

[20] J. C. Slater, Phys. Rev. **78**, 748 (1950).

[21] B. E. Vugmeister and M. D. Glinchuk, Rev. Mod. Phys. **62**, 993 (1990).

[22] S. Prosandeev, D. Wang, A. R. Akbarzadeh and L. Bellaiche, J. Phys.: Condens. Matter **27**, 223202 (2015).

[23] F. Chu, N. Setter, and A. K. Tagantsev, J. Appl. Phys. **74**, 5129 (1993).

[24] R. Hemphill, L. Bellaiche, A. Garćia, and D. Vanderbilt, Appl. Phys. Lett. **77**, 3642, (2000).

[25] P. K. Davies, M. A. Akbas, J. Phys. Chem. Solids **61**, 159 (2000); J. Am. Ceram. Soc., **80** 2933 (1997).

[26] M. A. Akbas and P. K. Davies, J. Am. Ceram. Soc., **83** 119 (2000).

[27] J. M. Cowley, Phys. Rev. **77**, 669 (1950); ibid. **120**, 1648 (1960).

[28] K. A. Mader and A. Zunger, Phys. Rev. B **51**, 10462 (1995).

[29] L. Bellaiche and A. Zunger, Phys. Rev. B **57**, 4425 (1998).

[30] A. M. George, J. Íñiguez, and L. Bellaiche, Phys. Rev. Lett. **91**, 045504 (2003).

[31] A. Al-Barakaty, S. Prosandeev, D. Wang, B. Dkhil, and L. Bellaiche, Phys. Rev. **91**, 214117 (2015).

[32] See Supplemental Material at [URL will be inserted by publisher] for more details about the effective Hamiltonian used here.

[33] J. Íñiguez and L. Bellaiche Phys. Rev. B **73**, 144109 (2006).

[34] K. M. Rabe and E. Cokayne, *First-Principles Calculations for Ferroelectrics: Fifth Williamsburg Workshop, edited by R. E. Cohen* (AIP, Woodbury, NY, 1998), p. 61.

[35] S. Prosandeev, D. Wang, and L. Bellaiche, Phys. Rev. Lett. **111**, 247602 (2013).

[36] D. Stauffer and A. Aharony, *Introduction to Percolation Theory* (Taylor & Francis, London, 1994).

[37] V. M. Ishchuk, V. N. Baumer, and V. L. Sobolev, J. Phys. Condens. Matter **17**, L177 (2005).

[38] N. Takesue, Y. Fujii, M. Ichihara, and H. Chen, Phys. Rev. Lett. **82**, 3709 (1999).

[39] I. P. Swainson, C. Stock, P. M. Gehring, Guangyong Xu, K. Hirota, Y. Qiu, H. Luo, X. Zhao, J.-F. Li, and D. Viehland, Phys. Rev. B **79**, 224301 (2009).

[40] A. M. George, J. Íñiguez, and L. Bellaiche, Phys. Rev. B **65** , 180301(R) (2002).

[41] Note that by symmetry, studying the Fourier transform of the y and z components of the local modes should give similar results than those depicted in Fig. 2b and corresponding to the Fourier transform of the x component of the local modes.

[42] These special q-points naturally depend on the size of the supercell, e.g. they become $2\pi(n_x, n_y, nz)/16a_{lat}$, with (n_x, n_y, nz) = (2,0,-2), (-2,0,2), (-2,2,0), (2,-2,0), (-2,-2,0), (2,2,0), (2,0,2), and (-2,0,-2), when investigating $16 \times 16 \times 16$ supercells.

[43] L. Bellaiche, J. Íñiguez, E. Cockayne, and B. P. Burton, Phys. Rev. B **75**, 014111 (2007).

[44] A. R. Akbarzadeh, S. Prosandeev, E. J. Walter, A. Al-Barakaty, and L. Bellaiche, Phys. Rev. Lett. **108**, 257601 (2012).

[45] D. Phelan, C. Stock, J. A. Rodriguez-Rivera, S. Chi, J. Leao, X. Long, Y. Xie, A. A. Bokov, Z.-G. Ye, P. Ganesh, and P. M. Gehring, PNAS 111, 1754 (2014).

FIG. 1. (color online) Predicted properties of PMN as a function of the chemical short-range order parameter α: (a) Dielectric permittivity; (b) inverse of the dielectric permittivity; (c) the T_B, T^*, and T_{depol} characteristic temperatures (see text); and (d) the averaged magnitude of the internal electric field, $E_{internal}$, acting on Pb ions. The inset in Figure 1d presents the dependence of T_B, T^*, and T_{depol} on the inverse of $E_{internal}$. The solid lines are guides for the eyes, and error bars result from the summation over 30 different configurations for each α.

FIG. 2. (color online) Computed microscopic properties of PMN as a function of the chemical short-range order parameter α, at 50K: (a) the average size s of the polar nanoregions (see text); and (b) the sum (over the eight specific q-points indicated in the text) of the magnitude of the Fourier transform of the x-components of the local modes. The left and right insets of Panel a are snapshots of the local modes' pattern for a single configuration corresponding to $\alpha = 0$ and 1, respectively, with the polar regions being delimited in red. The left and right insets of Panel b reports the $\theta_{x,x}$ quantity (see Eq. (2)) as averaged over the (001) planes of these two latter configurations, respectively. The solid lines are guides for the eyes, and error bars result from the summation over 30 different configurations for each α.

FIG. 3. (color online) Temperature dependence of the P_{ZFH-FC} polarization (see text) for the different investigated α parameters. The inset shows the magnitude of this polarization calculated at 10K, as a function of α. error bars result from the summation over 30 different configurations for each α.

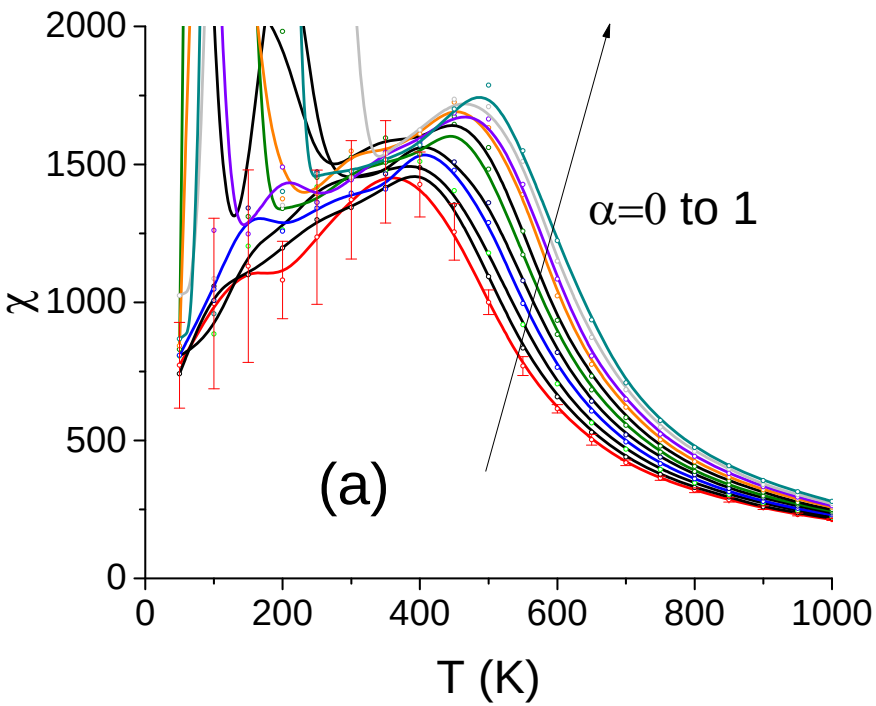
2000
1500
1000
500
0
χ
0
200
400
600
800
1000
T (K)
α=0 to 1
(a)

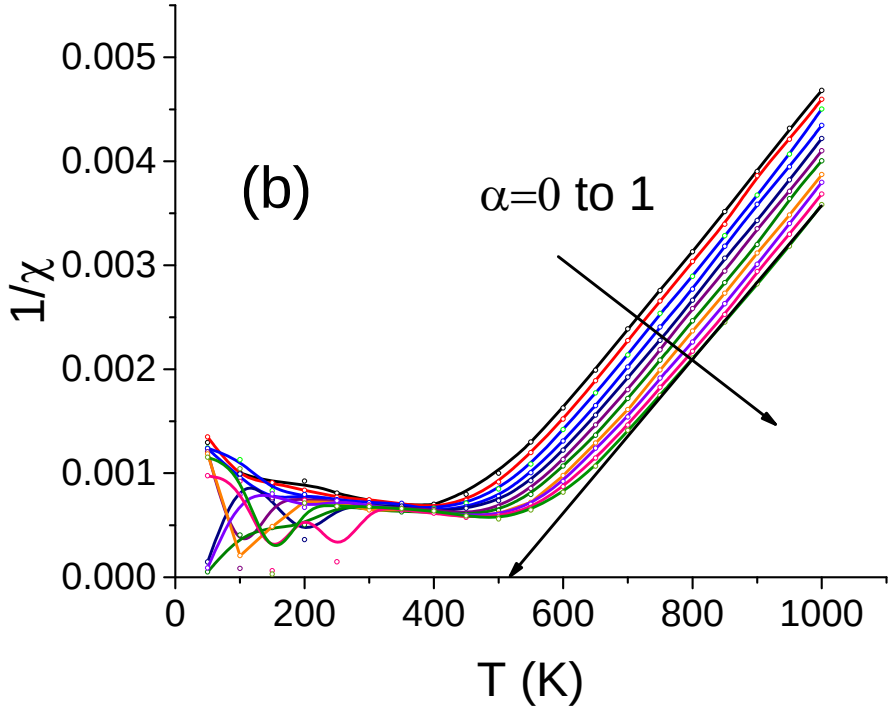
0.005
0.004
0.003
0.002
0.001
0.000
1/χ
0
200
400
600
800
1000
T (K)
(b)
α=0 to 1

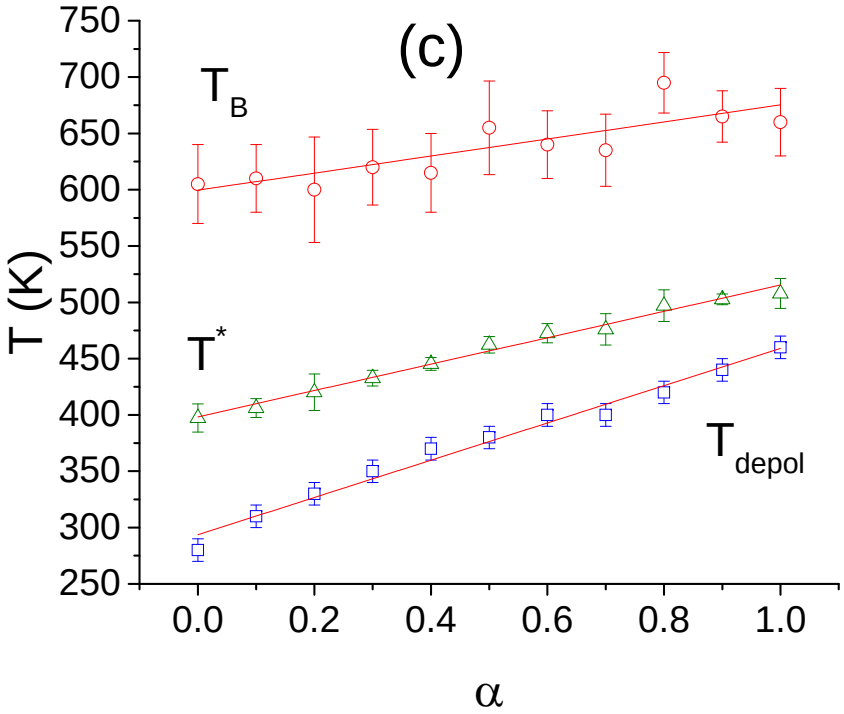
750
700
650
600
550
500
450
400
350
300
250
T (K)
0.0
0.2
0.4
0.6
0.8
1.0
α
(c)
T_B
T*
T_depol

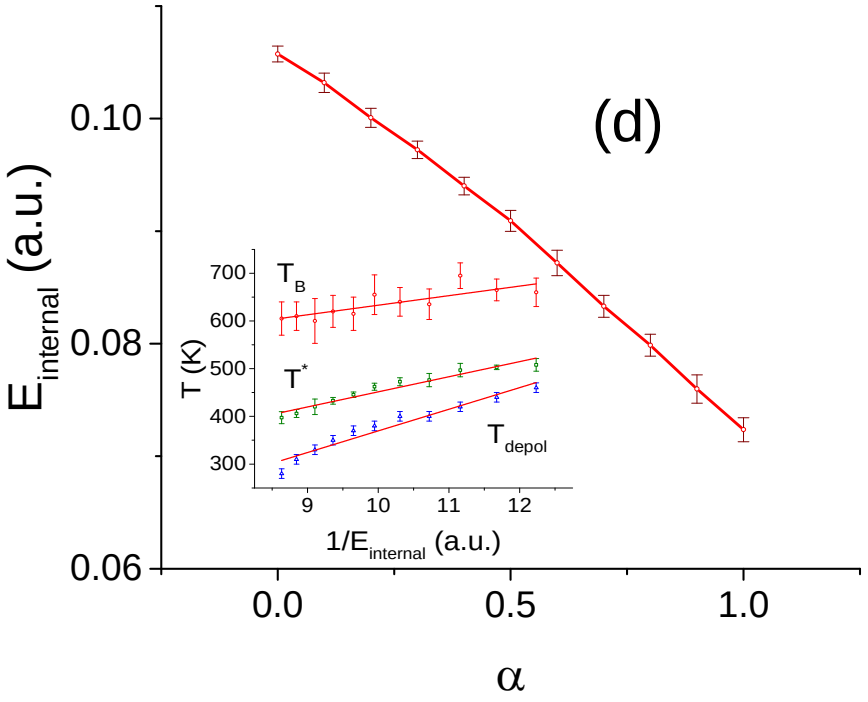
0.10
0.08
0.06
E_internal (a.u.)
0.0
0.5
1.0
α
(d)
700
600
500
400
300
T (K)
9
10
11
12
1/E_internal (a.u.)
T_B
T*
T_depol

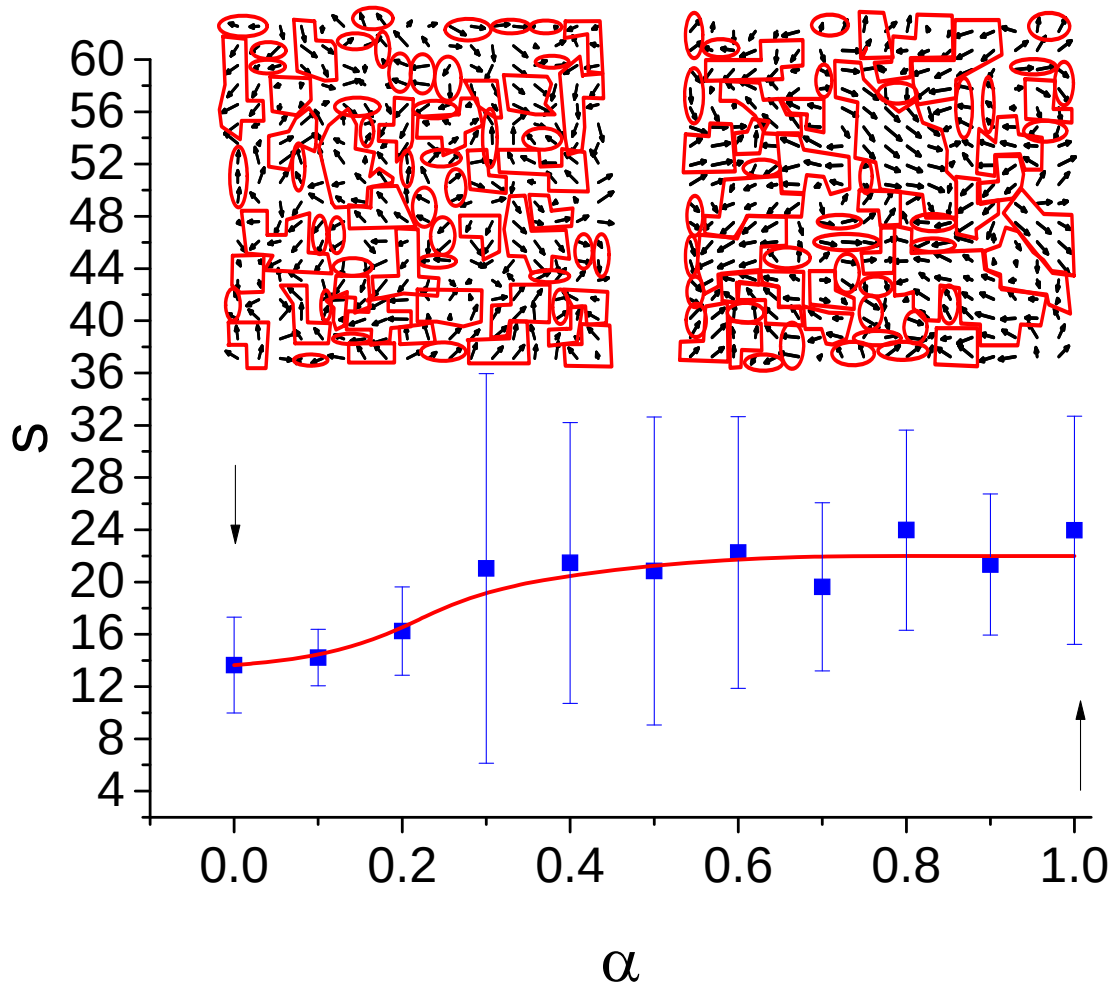
s
60
56
52
48
44
40
36
32
28
24
20
16
12
8
4
0.0
0.2
0.4
0.6
0.8
1.0
α

(a)

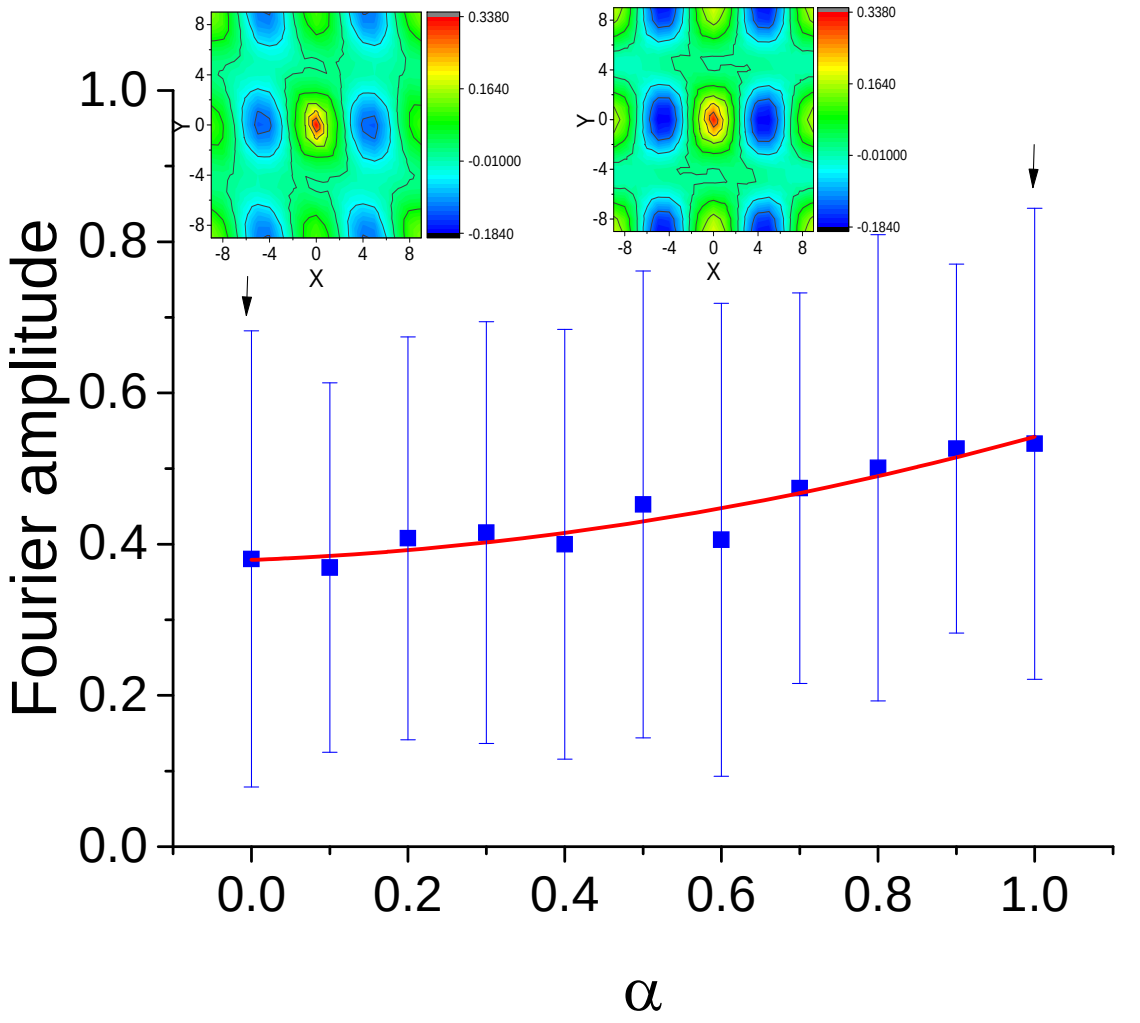
Fourier amplitude
1.0
0.8
0.6
0.4
0.2
0.0
0.0
0.2
0.4
0.6
0.8
1.0
α
Y
X
8
4
0
-4
-8
0.3380
0.1640
-0.01000
-0.1840

(b)

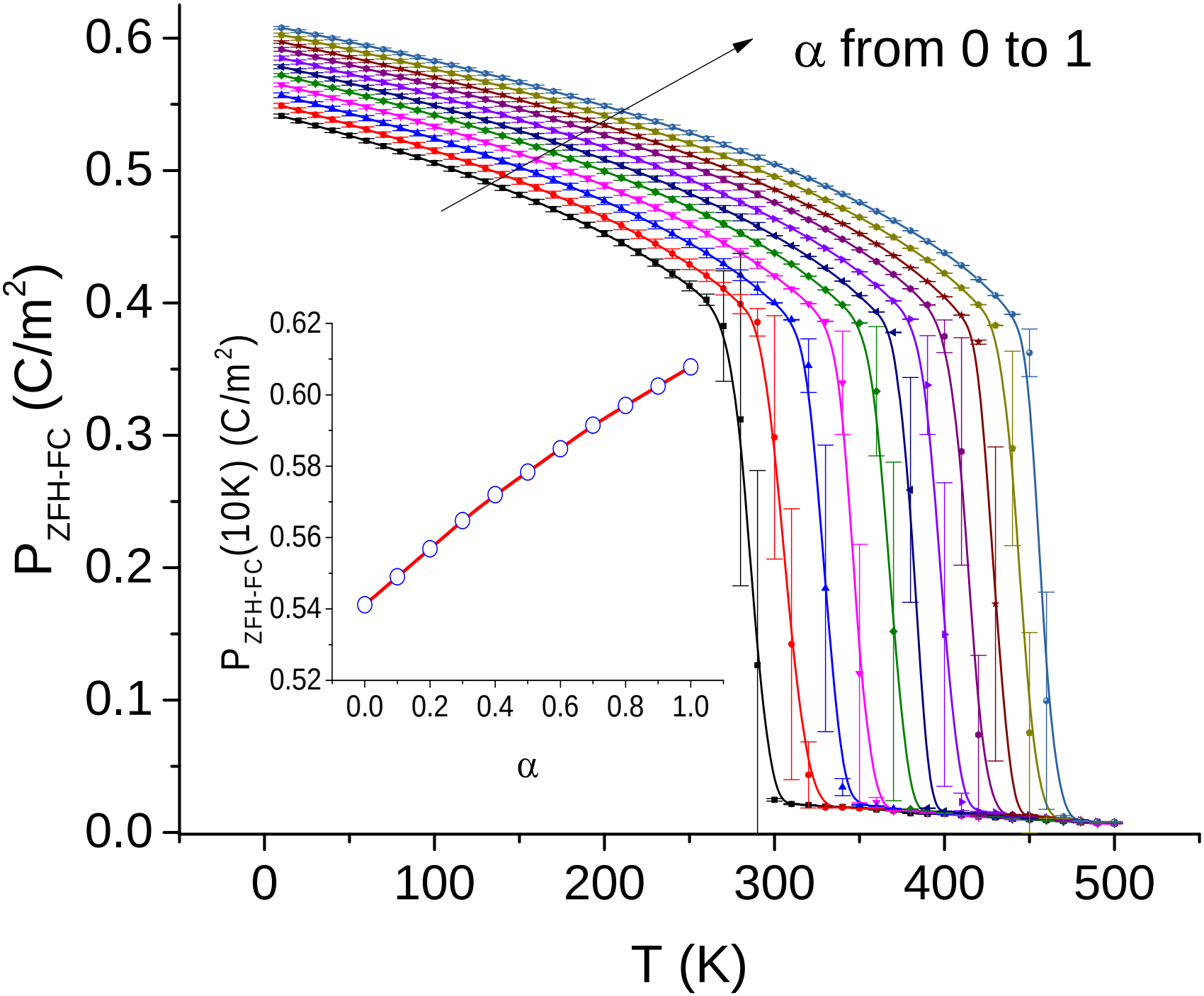
α from 0 to 1
P ZFH-FC (C/m2)
T (K)
0.0
0.1
0.2
0.3
0.4
0.5
0.6
0
100
200
300
400
500
P ZFH-FC(10K) (C/m2)
α
0.52
0.54
0.56
0.58
0.60
0.62
0.0
0.2
0.4
0.6
0.8
1.0